RSC Advances

PAPER

View Article Online
View Journal | View Issue

Cite this: RSC Adv., 2018, 8, 2552

Integration of the 3DOM Al/Co_3O_4 nanothermite film with a semiconductor bridge to realize a high-output micro-energetic igniter†

Zilong Zheng,[a] Wenchao Zhang, *[a] Chunpei Yu,[a] Guoqiang Zheng,[ab] Kefeng Ma,[c] Zhichun Qin,[a] Jiahai Ye [a] and Yimin Chao *[d]

Received 13th October 2017
Accepted 2nd January 2018

DOI: 10.1039/c7ra11293a

rsc.li/rsc-advances

Microigniters play an important role for the reliable initiation of micro explosive devices. However, the microigniter is still limited by the low out-put energy to realize high reliability and safety. Integration of energetic materials with microigniters is an effective method to enhance the ignition ability. In this work, a Al/Co_3O_4 nanothermite film with a three-dimensionally ordered macroporous structure was prepared by the deposition of nanoscale Al layers using magnetron sputtering on Co_3O_4 skeletons that are synthesized using an inverse template method. Both the uniform structure and nanoscale contact between the Al layers and the Co_3O_4 skeletons lead to an excellent exothermicity. In order to investigate the ignition properties, a micro-energetic igniter has been fabricated by the integration of the Al/Co_3O_4 nanothermite film with a semiconductor bridge microigniter. The thermite reactions between the nanoscale Al layer and the Co_3O_4 skeleton extensively promote the intensity of the spark, the length in duration and the size of the area, which greatly enhance the ignition reliability of the micro-energetic igniter. Moreover, this novel design enables the micro-energetic igniter to fire the pyrotechnic Zr/Pb_3O_4 in a gap of 3.7 mm by capacitor discharge stimulation and to keep the intrinsic instantaneity high and firing energy low. The realization of gap ignition will surely improve the safety level of initiating systems and have a significant impact on the design and application of explosive devices.

1. Introduction

Microelectromechanical systems (MEMS), as a cutting-edge technology in the 21st century, have been widely applied in physical, chemical, biological sensors and actuators.[1–5] Based on micromachining technology, MEMS devices, such as microcombustors, microgenerators and microthrusters,[6–8] possess the characteristics of miniaturization, microelectronic integration, and parallel fabrication with high precision. The semiconductor bridge (SCB), a kind of a MEMS product, is a typical ignition-transduction component in the system of initiators for explosive devices. The SCB has emerged as an initiator in military, civil and aerospace fields, since it is of higher instantaneity, higher safety and lower firing energy than those of conventional bridgewires.[9] However, a SCB, especially for a micro-SCB, just produces a very hot but low energy ignition source which lasts only for microseconds instead, so it makes providing a reliable ignition difficult. As a result, the primary contact ordnance material with SCB must be an extremely sensitive initiating explosive, which will drastically reduce the safety level.

The ignition ability of SCB has been improved by the exploitation of various trials including the introduction of a monolayer of a metal membrane[10,11] or nanothermites[12,13] in the bridge area. The exothermic reaction between the metal membrane and oxygen or nitrogen increases the output energy of SCB to some extent, but the amount of plasma is still too limited to achieve ignition in a gap.[10,11] Nanothermites (also called metastable intermolecular composites, MIC) are normally composed of the nanoscale aluminum fuel and metal oxides, such as Al/CuO, Al/Fe_2O_3, Al/MoO_3, Al/Bi_2O_3, Al/NiO.[14–18] In recent years, nanothermites, which are of a large contact area and short diffusion distance between fuel and oxidizer, have drawn so much attentions because of their low onset reaction temperature, high reaction rate and large heat release when compared with micro/macro-scale thermites.[19,20] Both multilayer nanolaminates (NLs)[21,22] and one-dimensional nanowires (NWs)[23–25] have been developed to synthesize nanothermites.

---

[a] School of Chemical Engineering, Nanjing University of Science and Technology, Nanjing 210094, China. E-mail: zhangwenchao@njust.edu.cn

[b] The 43rd Research Institute of CETC, Hefei 230088, China

[c] School of Environmental and Biological Engineering, Nanjing University of Science and Technology, Nanjing 210094, China

[d] School of Chemistry, University of East Anglia, Norwich NR4 7TJ, UK. E-mail: y.chao@uea.ac.uk

† Electronic supplementary information (ESI) available: Information on morphology images, comparisons for the sparks of the micro-energetic igniter at different voltages, analyses for the voltage–current curves, analyses for the input energy curves, DSC data, data of the ignition time and ignition energy. See DOI: 10.1039/c7ra11293a

When the nanothermites of the NLs structure are integrated on the bridge area, the SCB can produce great energy and high spark with the help of thermite reactions,[13,26] but the multilayer structure increases both the complexity and cost of the fabrication process and difficulty to scale up.[19] As for NWs, the Al and metal oxide possess such a large contact area for an intimate touch that their activation energy can be lowered quite a lot.[23–25] However, it is inevitable to have metal oxide film in such a microscale thickness within this structure of NWs that Al can be prevented from contacting very well with metal oxide film, thus dramatically affecting the application. Although the aforementioned studies suffered from certain defects, the introduction of nanothermites seems an efficient approach to tackle the low output energy of SCB.

A new class of nanothermites (*e.g.* Al/Fe_2O_3,[27] Al/Mn_2O_3,[28] Al/$NiFe_2O_4$ (ref. 29) and Al/NiO[30]) with a three-dimensionally ordered macroporous (3DOM) structure, in which a layer of Al is cladded on both the external and internal surfaces of the 3DOM metal oxide skeleton using an inverse template method, has been successfully developed.[31,32] Such interconnected porous structure can make the contact area between fuel and metal oxide increased so greatly as to get the mass and heat transfer distance dramatically reduced and result in a significant energy release as well. Furthermore, the *in situ* synthesis process of the 3DOM nanothermites is well compatible with the MEMS technology.[27] Based on the advantages listed above, the 3DOM nanothermites are quite promising to integrate into the bridge area of SCB, which will increase the output energy with a thermite reaction.

In this study, Al/Co_3O_4 nanothermites has been selected due to their high theoretical reaction heat of 4236.1 J g^{-1} and an adiabatic reaction temperature of 3201 K from the thermite reaction between Al and Co_3O_4, which is one of the most exothermic thermite reaction, as shown in eqn (1) below.[33]

$$8Al + 3Co_3O_4 \rightarrow 4Al_2O_3 + 9Co;\ \Delta H = 4236.1\ J\ g^{-1} \qquad (1)$$

Here, a 3DOM film of the Al/Co_3O_4 nanothermites has been prepared based upon a 3DOM Co_3O_4 skeleton, which will be integrated with various thicknesses of nanoscale Al layers by magnetron sputtering. Morphology, phase and exothermicity of the Al/Co_3O_4 nanothermites film have been investigated carefully using field emission scanning electron microscope (FE-SEM), fourier transform infrared spectroscopy (FTIR), X-ray diffraction (XRD), energy dispersive X-ray spectrum (EDS) and differential scanning calorimetry (DSC). Furthermore, the best-performing Al/Co_3O_4 nanothermites film within all achieved here is integrated with SCB to get a micro-energetic igniter, which can boost the ignition ability with the help of a thermite reaction. In addition, the promoted ignition performance, gap test and critical characteristic parameters of the micro-energetic igniter are discussed in detail.

2. Experimental section

2.1 Materials

Phenylethylene, sodium *p*-styrene sulfonate, sodium bicarbonate, sodium hydroxide, potassium persulfate, citric acid monohydrate, ethyl alcohol, ethylene glycol, hydrochloric acid, methanol and cobalt nitrate hexahydrate were all purchased from Sinopharm Chemical Reagent Co. Ltd. All the chemicals and materials was analytically pure and applied

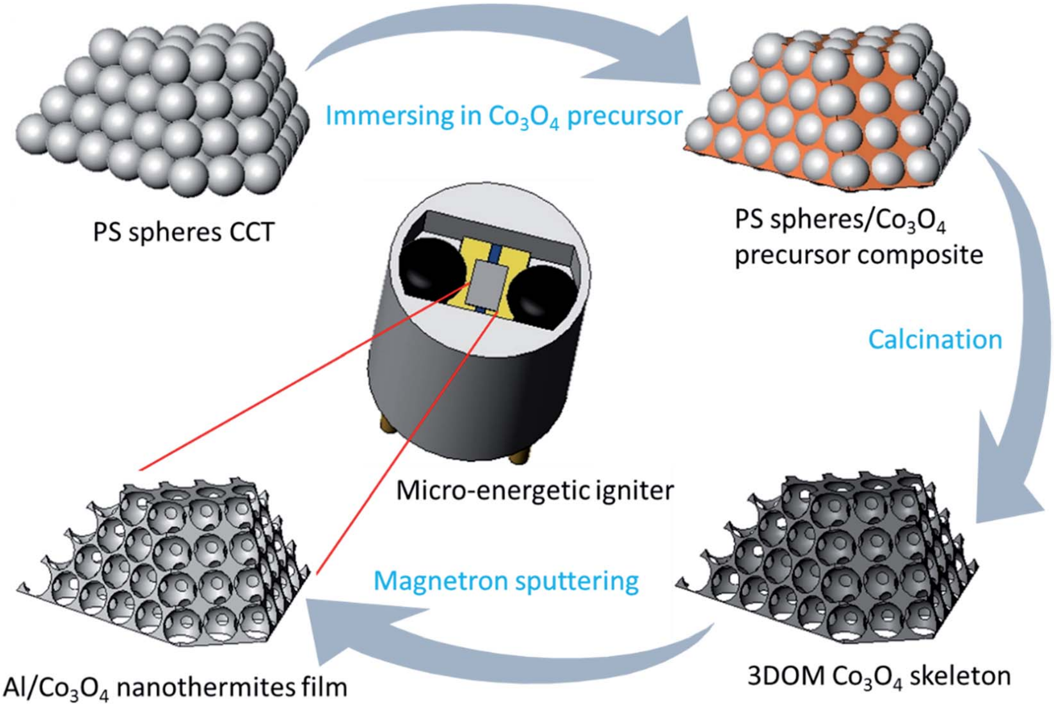

Fig. 1 The schematic for the preparation process of the Al/Co_3O_4 nanothermites film and micro-energetic igniter.

without further treatment. Deionized water was used in all experiments.

2.2 Preparations of the Al/Co_3O_4 nanothermites film

The preparation process of the Al/Co_3O_4 nanothermites film is shown in Fig. 1, whose specific procedures are described as follows. Monodispersed polystyrene (PS) spheres were prepared by the reported emulsifier-free polymerization technology.[27] The vertical deposition method was employed to prepare the colloidal crystal template (CCT) of PS spheres on the treated glass slide substrate.[34,35] The inverse template method was used to prepare the 3DOM Co_3O_4 skeleton as described in our previous work.[27] The difference here was just to alter the constituents of the precursor solution for a mixture of cobalt nitrate hexahydrate, citric acid, methanol and ethylene glycol. A nanoscale Al layer was then deposited onto the 3DOM Co_3O_4 skeleton by magnetron sputtering to synthesize the Al/Co_3O_4 nanothermites film. In order to obtain a desired heat release from the fabricated Al/Co_3O_4 nanothermites film, three kinds of films were prepared here for different aluminizing times of 10, 20 or 30 min, respectively.

2.3 Characterizations of Al/Co_3O_4 nanothermites film

The morphologies of the as-synthesized 3DOM Co_3O_4 skeleton and Al/Co_3O_4 nanothermites film were observed under FE-SEM (Hitachi, S-4800). XRD (Bruker, D8 Advance) patterns were collected to analyze the sample composition using a Cu Kα radiation ($\lambda = 0.15406$ nm) operated at 30 kV. FTIR (Thermo Fisher, Nicolet IS-10) spectra were acquired to confirm the sample composition in the range of 400–3000 cm^{-1} using potassium bromide tableting at room temperature. The EDS test was performed to determine the actual molar ratios of Al to Co_3O_4 in the nanothermites film. The heat releases of three kinds of the Al/Co_3O_4 nanothermites film were measured by DSC (Netzsch, STA449C) in the scan range from 100 to 900 °C under the N_2 atmosphere at a heating and flowing rate of 10 °C min^{-1} and 20 mL min^{-1}, respectively. Prior to XRD, FTIR, and DSC characterizations, the samples had to be scraped from the glass slide substrate.

2.4 Fabrications of micro-energetic igniters

The SCB chip based on silicon was prepared using a traditional procedure for a complementary metal oxide semiconductor (CMOS) including the silicon thermal oxidation, polysilicon define and electrode define, as detailedly described in the literature.[36] Phosphorus was doped into a polysilicon layer with a doping concentration of 7×10^{19} atoms cm^{-3} to achieve a resistance $1 \pm 0.2\ \Omega$. As shown in Fig. 2, the bridge area was formed in a typically double V shape.

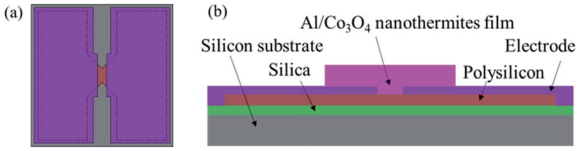

Fig. 2 (a) The schematic diagram of the SCB chip (a plan view). (b) The cross sectional view of the micro-energetic chip, the Al/Co_3O_4 nanothermites film which is coated onto the surface of the SCB chip.

After a SCB chip array was obtained, a stainless steel mask with many rectangular holes (0.7 × 1 mm) was covered on its surface. The rectangular holes were right on the bridge area, which made the bridge area exposure to the atmosphere to deposit the PS spheres. The size of the mask, whose thickness was 10 μm, should match with the SCB chip array. The as-covered SCB chip was then used as a substrate to prepare the Al/Co_3O_4 nanothermites film for a 20 min aluminization by the aforementioned method. The micro-energetic chip (cross sectional view shown in Fig. 2b) was finally obtained after the mask was moved.

Subsequently, the two chips were encapsulated in a ceramic chamber, as described as follows. Firstly, epoxy resin adhesive was used to combine the chip with ceramic chamber. Secondly, the bonding technology was adopted to connect the chip electrode and leg wire.[9] In addition, the bonding wire was protected with a silver slurry. Finally, the two chips were processed into the SCB microigniter and micro-energetic igniter, respectively, as shown in Fig. 1.

2.5 Ignition performance tests of the micro-energetic igniters

The two igniters were initiated by a capacitor discharge stimulation with the test circuit shown in Fig. 3 and test method described below. The tantalum capacitor was employed as an energy storage tool because of the advantages of small volume, small leakage current and high precision. First, the capacitor started charging when the switch joint 1 and 2 were connected together. Second, the switch was turned from joint 2 to 3 after a given voltage was attained in the capacitor. The sample (igniter) was ignited at the condition of a capacitor discharge stimulation. A high speed camera (Redlake HG-100K) was utilized to record the whole firing process. Meanwhile, a high-speed digital storage oscilloscope (LeCroy WaveSurfer44Xs)

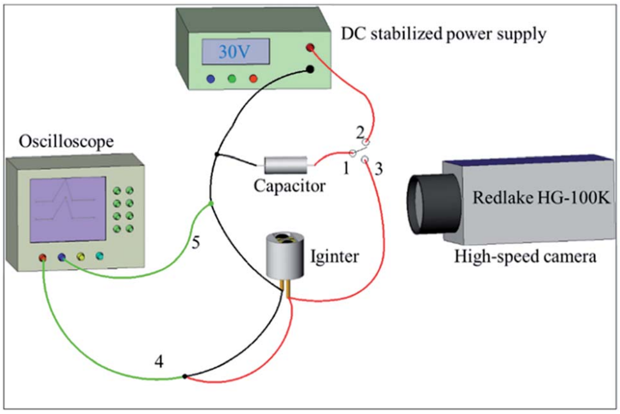

Fig. 3 The circuit diagram of the capacitor discharge test. 1, 2, 3-ignition switch; 4-oscilloscope voltage probe; 5-oscilloscope current probe.

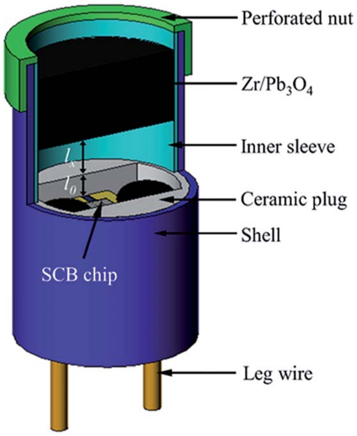

Fig. 4 The schematic of the gap test device.

was applied to acquire the current and voltage signals of the initiation process.

A gap test was conducted to illustrate the ignition ability of two igniters as shown in Fig. 4. The specific testing process was described below. Zr/Pb$_3$O$_4$ pyrotechnic (60 mg) was pressed into an inner sleeve with a pressing pressure of 60 MPa. The inner sleeve was put on the top of igniter and fixed by a perforated nut. The distance l_x was controlled by a mould with a location pillar. The distance l_0 from the chip surface to the top face of the ceramic plug was 0.7 mm. As a result, the ignition distance should be value of $l_0 + l_x$.

3. Results and discussion

3.1 Morphology, phase and exothermicity of the Al/Co$_3$O$_4$ nanothermites film

The monodispersed PS spheres are orderly distributed on a glass slide to form a CCT (eight layers) in Fig. 5a. The CCT presents a face-centered honeycomb structure with approximate hexagons because of their strong capillary adsorption forces.[37] The average diameter of the PS spheres is *ca.* 320 nm. After the Co$_3$O$_4$ precursor solution is infiltrated into the void of the PS spheres under the capillary force, the 3DOM Co$_3$O$_4$ skeleton will be formed in the complete removal of the PS spheres eliminated by a calcination in muffle furnace (Fig. 5b). It is obvious that the skeleton is a perfect reverse replication of the PS spheres in terms of structure. Pore walls are composed of double-layer nanoparticles with an average wall thickness of 37 nm. Due to some shrinkage from the CCT of PS spheres during the process of a calcination,[28] the pore diameter has reduced averagely upto *ca.* 190 nm, which is corresponding to a pore shrinkage rate of 40.6%. Since macrospores connect next to each other with a pore window, the whole space is interconnected so as to favor the deposition of the Al layer. The 3DOM Al/Co$_3$O$_4$ nanothermites film is manufactured after the Al layer is deposited on both external and internal surfaces of the 3DOM Co$_3$O$_4$ skeleton by means of magnetron sputtering. The FE-SEM image of the Al/Co$_3$O$_4$ nanothermites film after a 20 min aluminization shows that the ordered array is still maintained as shown in Fig. 5c. The average wall thickness increases to 137 nm but average pore size decreases to 83 nm. The Co$_3$O$_4$ skeleton is tightly coated by a nanoscale Al layer. The sectional view in Fig. 5c shows that the Al infiltrates into the 3DOM Co$_3$O$_4$ skeleton. When the aluminizing time decreases to 10 min, the pore windows still exist and the average wall thickness decreases to 95 nm (Fig. S1a in ESI†). However, pores are found out to be nearly clogged without an ordered array by an external Al layer when the aluminizing time increases to 30 min (Fig. S1b†).

The FTIR spectrum of Co$_3$O$_4$ skeleton exhibits two distinctive bands at *ca.* 552.4 and 656.4 cm^{-1}, both of which originate from the stretching vibrations of the metal–oxygen bonds (Fig. 6a). The band at 552.4 cm^{-1} should be related to the BOB$_3$ vibration in the spinel lattice, where B denotes the Co^{3+} ions in an octahedral position. The other band at 656.4 cm^{-1} results from the AOB$_3$ vibration, where A denotes Co^{2+} ions in a tetrahedral position.[38] The appearance of these two bands significantly confirms the formation of the Co$_3$O$_4$ spinel phase. No detected feature is associated with impurities, which indicates a high purity of the product. The XRD pattern of the 3DOM Co$_3$O$_4$ skeleton in 20 min aluminization (the black curve of Fig. 6b) shows diffraction peaks at 19.00°, 31.27°, 36.85°, 44.81°, 59.35° and 65.24°, which correspond to crystal planes (111), (220), (311), (400), (511) and (440) of the cubic spinel Co$_3$O$_4$ structure, respectively (JCPDS 42-1467). No other feature is observed either from the diffraction pattern, which reveals that a neat spinel phase is obtained. The XRD pattern of the Al/Co$_3$O$_4$ nanothermites film (the red curve of Fig. 6b) displays four diffraction

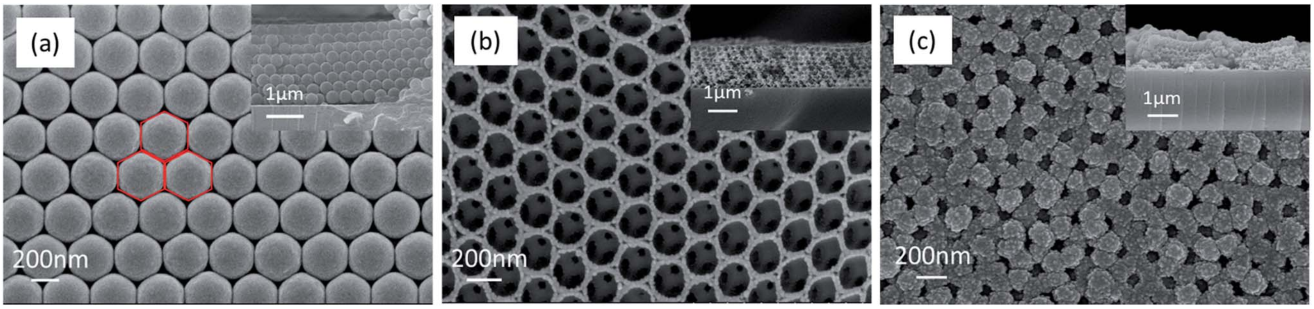

Fig. 5 The FE-SEM images of (a) the CCT of PS spheres, (b) the calcined 3DOM Co$_3$O$_4$ skeleton, and (c) the Al/Co$_3$O$_4$ nanothermites film for 20 min aluminization. The inset is section view.

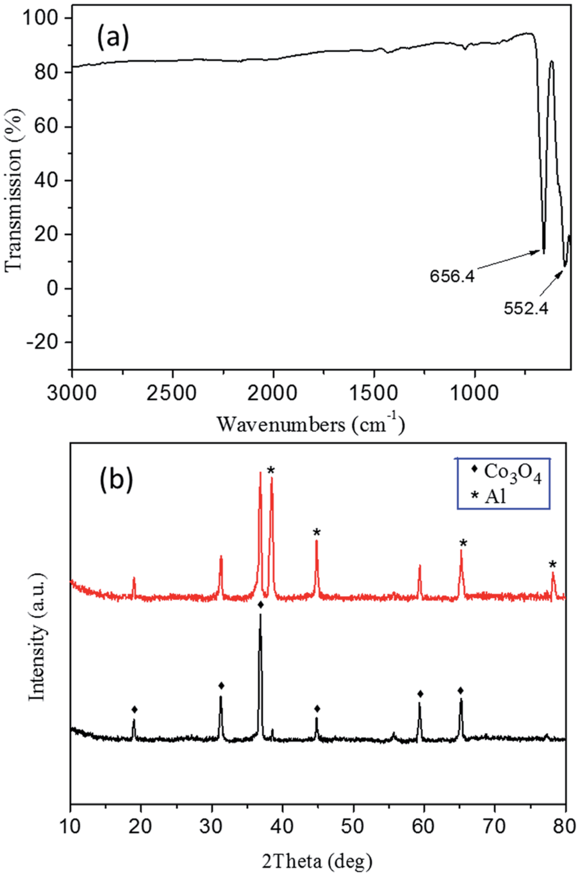

Fig. 6 (a) The FTIR spectrum of the 3DOM Co_3O_4 skeleton. (b) The XRD patterns of the 3DOM Co_3O_4 skeleton (black curve) and the Al/Co_3O_4 nanothermites film (red curve).

peaks at 38.47°, 44.74°, 65.13° and 78.22°, which are attributed to planes (111), (200), (220) and (311) of Al, respectively (JCPDS 04-0787). The characteristic peaks of the cubic spinel Co_3O_4 absolutely remain without any impurity peak so that no obvious pre-reaction happens during the deposition of Al.

The EDS test is used to determine the actual molar ratios of Al to Co_3O_4 in the nanothermites film. As shown in Fig. 7, besides the peaks of Al and Co, the Si peak and Au peak are also found from the glass substrate and the process of gold spraying for improvement in conductivity. According to the results of EDS, the atomic percentages of Al and Co element in the Al/Co_3O_4 nanothermites film at different aluminizing times of 10, 20 and 30 min are 43.40%, 62.08%, 86.95% and 56.60%, 37.92%, 13.05%, respectively. As a result, the molar ratios of Al to Co_3O_4 in the nanothermites film are 2.30, 4.91 and 19.99 at different aluminizing times of 10, 20 and 30 min. The results are listed in Table 1, which show that the molar ratios of Al to Co_3O_4 increases with increasing aluminizing time. The stoichiometric ratio of Al and Co_3O_4 is 2.67, so Al is inadequate for a 10 min aluminization, slightly excessive for a 20 min and severely excessive for a 30 min aluminization, all of which are consistent with the characterizations of SEM.

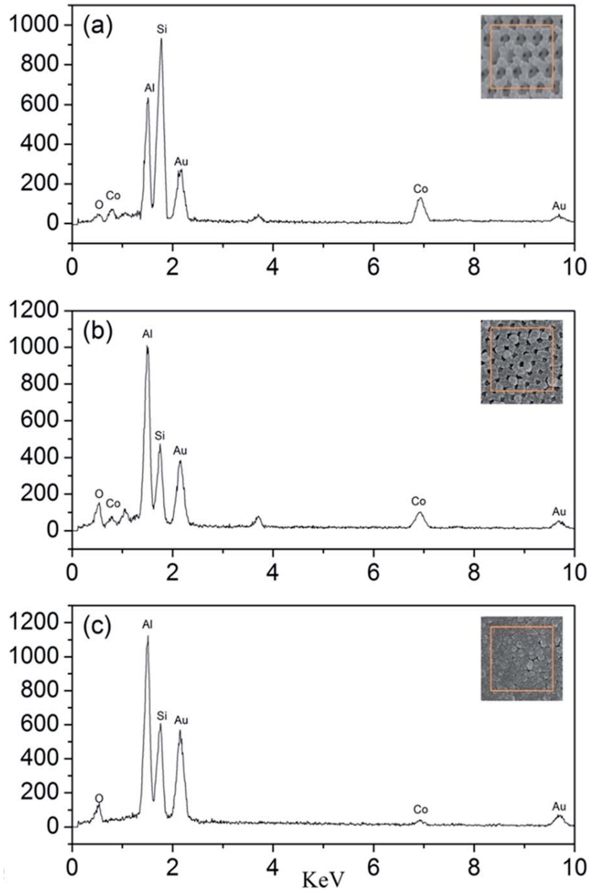

Fig. 7 The EDS patterns of the Al/Co_3O_4 nanothermites film at different aluminizing times of (a) 10 min; (b) 20 min, (c) 30 min.

Fig. 8 shows the DSC curves of the Al/Co_3O_4 nanothermites film at different aluminizing times of 10, 20 and 30 min, respectively. The 10 min aluminization just leads to a small exothermic peak with a heat release of 782.4 J g^{-1} (see Table S1†), so it seems to be seriously inadequate amount of the deposited Al. Three obvious peaks emerge at 569 °C, 679 °C and 741 °C for the nanothermites film of 20 min aluminization in Fig. 8. The onset temperature of the first peak is 431 °C, which is far below the plasma temperature of SCB (~5230 K),[9] so the nanothermites is able to be ignited in theory. Furthermore, a heat release of 1325.9 J g^{-1} (see Table S1†) for the first exothermic peak is larger than that for the nanothermites of 10 min aluminization. It further confirms that 10 min is inadequate for aluminization. A relatively small and obvious endothermic peak at 679 °C is corresponding to the melting process

Table 1 Elemental compositions of the Al/Co_3O_4 nanothermites film at different aluminizing times

Aluminizing time (min)	Atomic percentage of the elements (%)		Molar ratio of Al to Co_3O_4
	Al	Co	
10	43.40	56.60	2.30
20	62.08	37.92	4.91
30	86.95	13.05	19.99

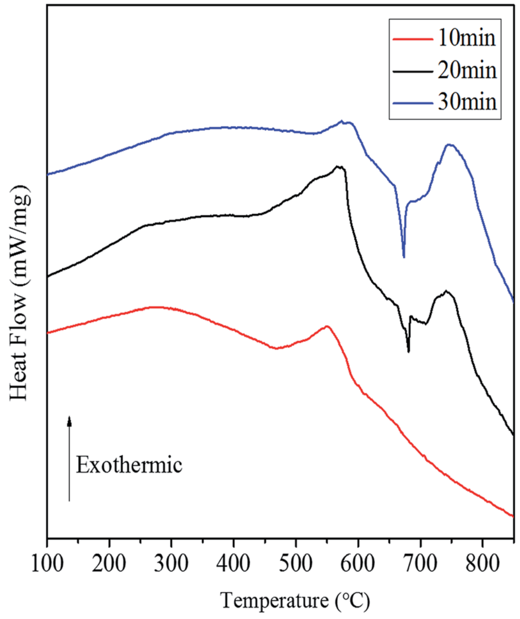

Fig. 8 The DSC curves of the Al/Co_3O_4 nanothermites film at different aluminizing times of (a) 10 min; (b) 20 min; (c) 30 min.

of Al according to a previous study.[28] The third exothermic peak at 741 °C with an onset temperature of 708 °C and a heat release of 498.0 J g^{-1} possesses a steeper upslope namely for a rapider thermite reaction rate than that of first exothermic peak. Two reasons may contribute to such a fast reaction rate of the second exothermic peak. On the one hand, a high temperature for the second exothermic peak undoubtedly can accelerate the thermite reaction rate. On the other hand, before the nanoscale Al layer melts, its relatively small contact area with Co_3O_4 in solid state (see Fig. 9) is supposed to result in a slow upslope curve. However, since the solid-state 3DOM Co_3O_4 skeleton is surrounded by the liquid Al above the temperature of 685 °C, each Co_3O_4 nanoparticle surface is a reaction interface as shown in Fig. 9. It is undoubted that the reaction interfaces of the liquid-state Al with the Co_3O_4 nanoparticles should be much greater than that of the solid-state Al. Therefore, the exothermic reaction rate is expected to accelerate after Al melts. When the aluminizing time extends to 30 min, only a small exothermic peak appears before Al melts, which is smaller than that of the nanothermites for 20 min aluminization. This can be attributed to excessive Al (Fig. S1b†) for a complete fill-up in the space of the film skeleton. If the Al layer is too thick, it will restrain the solid–solid reaction between Al and Co_3O_4 based upon the results of a previous study.[28] When Al starts melting, the reaction will be accelerated remarkably with high intensity for a steep exothermic peak in the DSC thermography, which can also be explained as mentioned above. In order to study the effect of the aluminizing time on the DSC results, the heat release before and after Al melts, and total heat release of the Al/Co_3O_4 nanothermites film are listed in the Table S1.† When the aluminizing time is 20 min, the exothermic performance of the nanothermites film is favorable with a heat release upto 1740.4 J g^{-1}. The maximum heat release accounts for 49.0% of the actual theoretical value of 3548.9 J g^{-1}.

3.2 Ignition performances of micro-energetic igniters

On the basis of the above studies, a novel micro-energetic chip has been realized by the replacement of the glass slide substrate with a SCB chip array. The micro-energetic igniter is manufactured by the encapsulation of a micro-energetic chip into a ceramic chamber, as shown by a schematic illustration in Fig. 1. The SCB microigniter is also fabricated without integrated nanothermites using the same encapsulating method to compare with the micro-energetic igniter. In order to study the effects of nanothermites film on SCB, the two igniters have been stimulated by a capacitor discharge to be recorded with fire images by a high-speed camera. A series of high-speed photography images are shown for the SCB microigniters (left) and micro-energetic igniters (right) which are discharged in 47 μF and different voltages (30, 40, 50 and 60 V) (Fig. 10). The point-in-time of each first collected picture is considered as an initiation of two igniters. The sampling frequency is 30 000 frames per second in test with no more than 33.33 μs of the

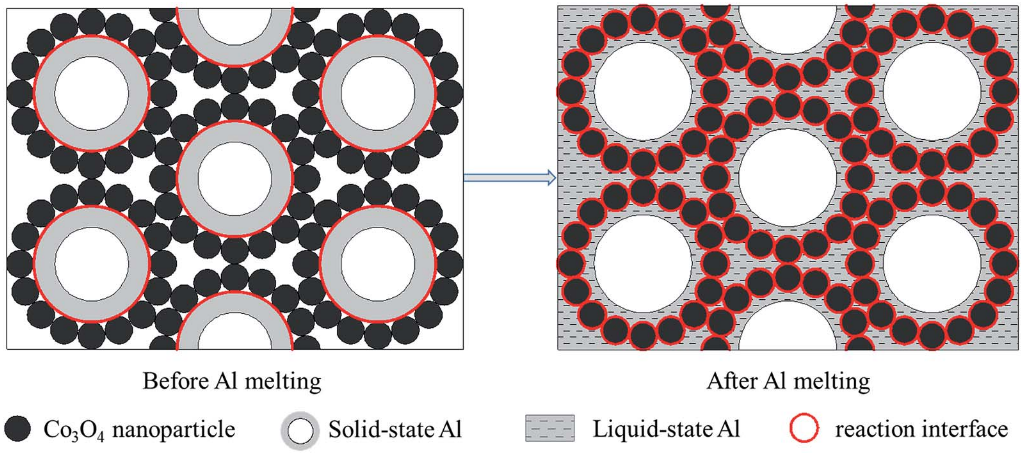

Fig. 9 The schematic illustrations for exaggerated perspectives to demonstrate reaction interfaces before and after Al melts.

maximum error. In comparisons of the images in Fig. 10b with 6f, the maximum spark height of the micro-energetic igniter is 6.3 mm, which is 2.6 mm higher than the maximum value of the plasma generated by the SCB microigniter. Not only its spark duration of 66.67 μs is longer, but also spark area is larger than the corresponding value of the SCB microigniter. Moreover, similar comparative results can be found at all other voltages. The videos of two igniters, which are discharged in 47 μF/50 V, are recorded in the ESI.† At this discharge voltage, the maximum spark height in this work is estimated about 8 mm, which is 0.4 mm higher than that of similar work in the same ignition condition.[39] However, the spark duration is shorter than the value of that work. The main reason for this result is that the self-propagating reaction does not occur for the Al/Co_3O_4 nanothermites film.

The boosted spark should be attributed to the integration of the Al/Co_3O_4 nanothermites film on the SCB bridge area. The film is ignited to form flying particles under the action of a weak shock wave from the high temperature plasma that is generated by the SCB. Subsequently, the thermite reaction of Al with the flying particles of Co_3O_4 in the air produces a large spark and great energy. In addition, both the spark height and duration increase with increasing voltage, as analyzed detailedly in the ESI.†

In order to further verify the ignition abilities of two igniters, gap tests have been conducted to fire the pyrotechnic Zr/Pb_3O_4 using a capacitor discharge stimulation. The high temperature plasma generated by a SCB fires pyrotechnic through micro-convection in accordance with the ignition mechanism,[36] but this process is strongly influenced by the gap size. After the Al/Co_3O_4 nanothermites film are integrated onto the surface of SCB, the thermite reaction between Al and the flying particles of Co_3O_4 in the air uplifts the output energy. The initiation gap of the micro-energetic igniter reaches to 3.7 mm, whereas the SCB microigniter is able to initiate the pyrotechnic when the gap is not more than 0.7 mm. It indicates that the ignition ability of the micro-energetic igniter is stronger than that of SCB microigniter. As an enhanced ignition-transduction component, the micro-energetic igniter is promising to be applied in a gap ignition system to improve the safety level.

In order to investigate the instantaneity and ignition energy of the igniters, the voltage and ignition energy (calculated from current) of two igniters during the process of ignition have been recorded by a high-speed digital storage oscilloscope. The ignition time is defined by the second voltage peak where the plasma starts to form (see Fig. S2 of ESI†) while the ignition energy is calculated by the formula of $E = \int_0^t UI\mathrm{d}t$.[40] Corresponding data are listed in Table S2 and S3,† respectively, and plotted in Fig. 11. Here, the ignition energies of the two igniters are almost same in Fig. 11b, which should be contributed to the fixed size, density and atomic weigh of the polysilicon bridge area. As a consequence, the liquefaction and vaporization energies are not expected to be changed too much.[41] Therefore, the ignition energy of the micro-energetic igniter is supposed not to be affected by the nanothermites film and discharging voltage. The ignition time curves of the two igniters are almost too close to

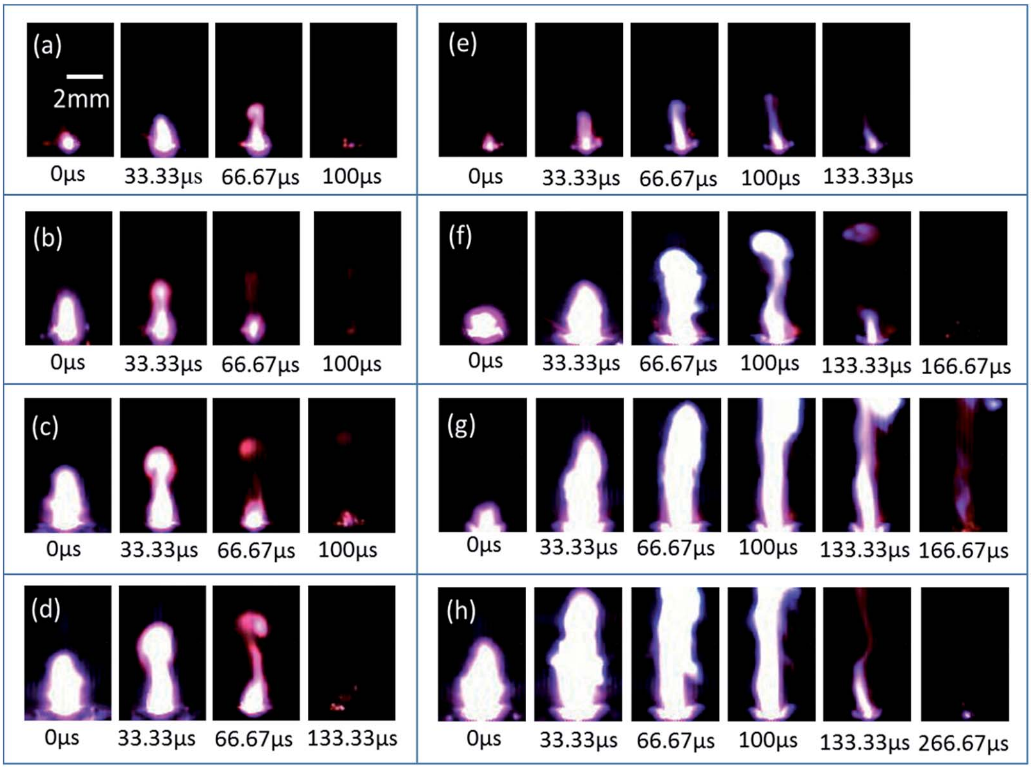

Fig. 10 The high-speed photography images of the SCB igniters (left frame) and micro-energetic igniters (right frame), which are discharged in 47 μF at (a, e) 30 V, (b, f) 40 V, (c, g) 50 V and (d, h) 60 V, respectively. In the (g) and (h) images, the sparks are too high to show entirely.

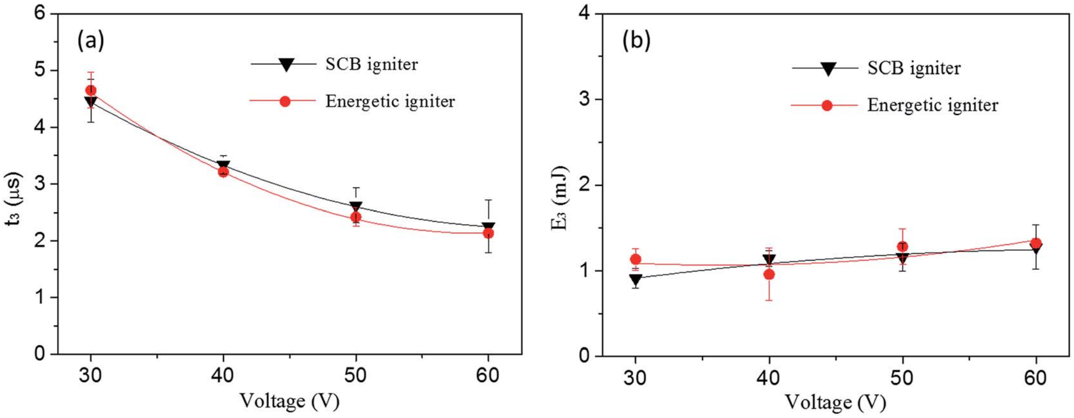

Fig. 11 (a) The ignition time and (b) corresponding ignition energy of the SCB igniter and micro-energetic igniter discharged in 47 μF at 30, 40, 50 and 60 V, respectively.

overlap in Fig. 11a. It indicates that the Al/Co_3O_4 nanothermites film has no distinct influence on the high instantaneity and low firing energy of the micro-energetic igniter.

4. Conclusions

The Al/Co_3O_4 nanothermites film has been successfully prepared to be a uniform and interconnected 3DOM structure, in which a 3DOM Co_3O_4 skeleton is densely coated by a nanoscale Al layer. Owing to a large contact area and short mass transfer distance between fuel and metal oxide, the nanothermites lead to a low onset temperature, which makes it possible to be ignited by a hot plasma. The 20 min aluminization could be favorable for the ratio adjustment of Al in order to optimize the exothermicity of the nanothermites film. Based upon the excellent Al/Co_3O_4 nanothermites, we have developed a novel micro-energetic igniter by the integration of the Al/Co_3O_4 nanothermites film with a SCB chip. The thermite reaction of the nanoscale Al layer with the Co_3O_4 skeleton makes the spark height, duration and area of micro-energetic igniter all much greater than these of the corresponding SCB micro-igniter. As a result, the micro-energetic igniter can fire Zr/Pb_3O_4 in a large gap of 3.7 mm. Furthermore, the high instantaneity and low firing energy of the micro-energetic igniter are still maintained under the integration of the Al/Co_3O_4 nanothermites film. Such strengthened ignition technology is suitable for a noncontact ignition and quite promising to be applied in military and civilian fields, especially in MEMS systems, *e.g.* micropropulsion and microcombustor devices.

Conflicts of interest

The authors declare that they have no conflict of interest.

Acknowledgements

This work was supported by the National Natural Science Foundation of China (Grant numbers 51576101); National Science Foundation of Jiangsu Province of China (grant numbers BK20141399, 20141223); the Fundamental Research Funds for the Central Universities (grant numbers 30915012101); and the Priority Academic Program Development of Jiangsu Higher Education Institutions.

References

1 G. J. Snyder, J. R. Lim, C. K. Huang and J. P. Fleurial, *Nat. Mater.*, 2003, **2**, 528–531.
2 J. L. Arlett, E. B. Myers and M. L. Roukes, *Nat. Nanotechnol.*, 2011, **6**, 203–215.
3 H.-P. Phan, D. V. Dao, L. Wang, T. Dinh, N.-T. Nguyen, A. Qamar, P. Tanner, S. Dimitrijev and Y. Zhu, *J. Mater. Chem. C*, 2014, **3**, 1172–1176.
4 L. C. Huang, W. Rieutort-Louis, A. Gualdino, L. Teagno, Y. Z. Hu, J. Mouro, J. Sanz-Robinson, J. C. Sturm, S. Wagner, V. Chu, J. P. Conde and N. Verma, *IEEE J. Solid-State Circuits*, 2015, **50**, 1002–1015.
5 W. Yang, D. Jiang, K. Y. K. Chua, Z. Dan and J. Pan, *Chem. Eng. J.*, 2015, **274**, 231–237.
6 W. M. Yang, S. K. Chou, C. Shu, H. Xue and Z. W. Li, *J. Microelectromech. Syst.*, 2004, **13**, 851–856.
7 D. H. Lewis, S. W. Janson, R. B. Cohen and E. K. Antonsson, *Sens. Actuators, A*, 2000, **80**, 143–154.
8 J. L. Wan, A. W. Fan, H. Yao and W. Liu, *Energy Convers. Manage.*, 2015, **96**, 605–612.
9 D. A. Benson, M. E. Larsen, A. M. Renfund, W. M. Trott and J. R. W. Biekes, *J. Appl. Phys.*, 1987, **62**, 1622–1632.
10 B. Martinez-Tovar and M. C. Foster, *U.S. pat.*, 20080017063A1, 2008.
11 W. Fahey, *Presented in part at the 37th Joint Propulsion Conference and Exhibit*, Salt Lake City, UT, U.S.A., July, 2001.
12 K. L. Zhang, C. Rossi, M. Petrantoni and N. Mauran, *J. Microelectromech. Syst.*, 2008, **17**, 832–836.
13 G. Taton, D. Lagrange, V. Conedera, L. Renaud and C. Rossi, *J. Micromech. Microeng.*, 2013, **23**, 105009.
14 L. Glavier, G. Taton, J. M. Ducere, V. Baijot, S. Pinon, T. Calais, A. Esteve, M. D. Rouhani and C. Rossi, *Combust. Flame*, 2015, **162**, 1813–1820.

15 J. L. Cheng, H. H. Hng, Y. W. Lee, S. W. Du and N. N. Thadhani, *Combust. Flame*, 2010, **157**, 2241–2249.

16 L. Marin, C. E. Nanayakkara, J.-F. Veyan, B. Warot-Fonrose, S. Joulie, A. Esteve, C. Tenailleau, Y. J. Chabal and C. Rossi, *ACS Appl. Mater. Interfaces*, 2015, **7**, 11713–11718.

17 D. X. Zhang and X. M. Li, *J. Phys. Chem. A*, 2015, **119**, 4688–4694.

18 L. J. Qin, N. Yan, J. G. Li, H. X. Hao, F. Q. Zhao and H. Feng, *RSC Adv.*, 2017, **7**, 7188–7197.

19 X. Zhou, M. Torabi, J. Lu, R. Q. Shen and K. L. Zhang, *ACS Appl. Mater. Interfaces*, 2014, **6**, 3058–3074.

20 Y. Yang, D. G. Xu and K. L. Zhang, *J. Mater. Sci.*, 2012, **47**, 1296–1305.

21 M. Bahrami, G. Taton, V. Conedera, L. Salvagnac, C. Tenailleau, P. Alphonse and C. Rossi, *Propellants, Explos., Pyrotech.*, 2014, **39**, 365–373.

22 C. Lanthony, M. Guiltat, J. M. Ducere, A. Verdier, A. Hemeryck, M. Djafari-Rouhani, C. Rossi, Y. J. Chabal and A. Esteve, *ACS Appl. Mater. Interfaces*, 2014, **6**, 15086–15097.

23 K. L. Zhang, C. Rossi, G. A. A. Rodriguez, C. Tenailleau and P. Alphonse, *Appl. Phys. Lett.*, 2007, **91**, 113117.

24 Y. Ohkura, S.-Y. Liu, P. M. Rao and X. L. Zheng, *Proc. Combust. Inst.*, 2011, **33**, 1909–1915.

25 Z. J. Liu, B. Hu, D. L. Li, P. Zhu, Y. H. Ye and R. Q. Shen, *Eur. Phys. J.: Appl. Phys.*, 2015, **72**, 93–103.

26 J. Xu, Y. Tai, C. Ru, J. Dai, Y. Ye, R. Shen and P. Zhu, *ACS Appl. Mater. Interfaces*, 2017, **9**, 5580–5589.

27 W. C. Zhang, B. Q. Yin, R. Q. Shen, J. H. Ye, J. A. Thomas and Y. M. Chao, *ACS Appl. Mater. Interfaces*, 2013, **5**, 239–242.

28 G. Q. Zheng, W. C. Zhang, R. Q. Shen, J. H. Ye, Z. C. Qin and Y. M. Chao, *Sci. Rep.*, 2016, **6**, 22588.

29 L. M. Shi, W. C. Zhang, J. Cheng, C. P. Yu, R. Q. Shen, J. H. Ye, Z. C. Qin and Y. M. Chao, *RSC Adv.*, 2016, **6**, 93330–93334.

30 C. Yu, W. Zhang, R. Shen, X. Xu, J. Cheng, J. Ye, Z. Qin and Y. Chao, *Mater. Des.*, 2016, **110**, 304–310.

31 Y. Chu and Q. M. Pan, *ACS Appl. Mater. Interfaces*, 2012, **4**, 2420–2425.

32 Y. Wang, H. X. Dai, J. G. Deng, Y. X. Liu, Z. X. Zhao, X. W. Li and H. Arandiyan, *Chem. Eng. J.*, 2013, **226**, 87–94.

33 S. H. Fischer and M. C. Grubelich, *Presented in part at the Twenty-Fourth International Pyrotechnics Seminar*, Monterey, CA, July, 1998.

34 D. J. Norris, E. G. Arlinghaus, L. Meng, R. Heiny and L. E. Scriven, *Adv. Mater.*, 2004, **16**, 1393–1399.

35 Z. Q. Tong, J. Hao, K. Zhang, J. P. Zhao, B. L. Su and Y. Li, *J. Mater. Chem. C*, 2014, **2**, 3651–3658.

36 E. Zvulun, G. Toker, V. T. Gurovich and Y. E. Krasik, *J. Appl. Phys.*, 2014, **115**, 203301.

37 Z. Cheng, W. B. Russel and P. M. Chaikin, *Nature*, 1999, **401**, 893–895.

38 R. H. Wang, C. H. Xu, J. Sun, Y. Q. Liu, L. Gao and C. C. Lin, *Nanoscale*, 2013, **5**, 6960–6967.

39 J. B. Xu, Y. Tai, C. B. Ru, J. Dai, Y. Shen, Y. H. Ye, R. Q. Shen and S. Fu, *J. Appl. Phys.*, 2017, **121**, 113301.

40 J.-U. Kim, C.-O. Park, M.-I. Park, S.-H. Kim and J.-B. Lee, *Phys. Lett. A*, 2002, **305**, 413–418.

41 K.-N. Lee, M.-I. Park, S.-H. Choi, C.-O. Park and H. S. Uhm, *Sens. Actuators, A*, 2002, **96**, 252–257.